Materials Physics and Mechanics 32 (2017) 278-287 Received: November 2, 2017

ELASTOMER COMPOSITES BASED ON FILLER WITH NEGATIVE COEFFICIENT OF THERMAL EXPANSION: EXPERIMENTS AND NUMERICAL SIMULATIONS OF STRESS-STRAIN BEHAVIOUR

S.N. Shubin[1*], A.G. Akulichev[2], A.B. Freidin[1,3,4]

[1]Institute for Problems in Mechanical Engineering of Russian Academy of Science, Saint-Petersburg, Russia

[2]Norwegian University of Science and Technology, Trondheim, Norway

[3] Peter the Great Saint-Petersburg Polytechnic University, Saint-Petersburg, Russia

[4]Saint-Petersburg University, Saint-Petersburg, Russia

*e-mail: ShubinSN@gmail.com

Abstract. We consider composites made of hydrogenated nitrile butadiene rubber (HNBR) and particles of zirconium tungstate (ZrW_2O_8). We focus on finite element (FE) modelling of a finite-strain mechanical behaviour of the composite and validation of the numerical simulation against experiments. Based on examination of composite microstructure by scanning electron microscope and optical analysis of particle images, realistic representative volume elements (RVE) of microstructure are generated taking into consideration the particles circularity and size distributions. Then FE simulations are performed to study the influence of the microstructure and matrix-filler interface conditions on the mechanical properties of the composites. It is assumed that the mechanical behaviour of rubber is non-linear, while the tungstate particles are modelled by a linear elastic material. The FE simulations reproduce uniaxial compression tests. Two types of interface condition between matrix and particles are simulated: a perfect adhesion and absence of adhesion. Corresponding stress-strain curves are constructed. Comparison with experiments shows that the real stress-strain curves for pre-loaded samples path within intervals given by the modelling, i.e. pre-loading leads to partial damage of bonding between matrix and particles.

Keywords: elastomer composite, representative volume element, effective stress-strain curve, damage, debonding.

1. Introduction

In the paper, the mechanical behaviour of composites consisting of hydrogenated nitrile butadiene rubber (HNBR) and particles of zirconium tungstate (ZrW_2O_8) that exhibits negative coefficient of thermal expansion (CTE) is studied. The fillers with low thermal expansivity provide an opportunity to reduce the thermal shrinkage of the composite in cooling [1, 2]. It is especially relevant in sealing applications for equipment operated at low temperatures. It is known that CTE of rubber is at least an order of magnitude higher than that of steel (see, for instance, [3]). Due to this fact, an elastomer seal compressed in its groove at room temperature may lose interference with the mating part after cooling and, thus, form a leak path for the contained fluid [1, 4]. In the previous work [1], we investigated analytically based on assumptions of linear elasticity how the volume fraction and the shape of the filler particles affect thermo-elastic properties, and, thus, the sealing performance of the composite. We also analysed the micro-stress at the particle-matrix interface caused by the seal squeeze and showed

that debonding may occur.

It is well known, that damage at the filler-matrix interface might significantly impact the mechanical behaviour of composites. This problem has been studied experimentally, analytically and numerically by many researchers. Particularly, particle-matrix debonding is experimentally investigated for elastomeric specimens containing one (e.g. [5]) or an array of rigid spherical particles (e.g. [6, 7, 8]). Analytical treatments provide a suitable approach to model debonding for idealized relatively simple composite microstructure and have well-known limits related to the non-linear behaviour of elastomer matrix, large deformation, high volume fraction, etc. A review of analytical modelling approaches together with a discussion on the limits of models could be found in [9]. On the other hand, numerical simulation allows to bridge the gap between analytical models and the real behaviour of composites with complicated microstructure (see an interesting discussion of this question in [10], where comparison between two methods is given). In some studies, a plane-strain assumption is used to model composites with circular particles distributed periodically (e.g. [11]) or randomly (e.g. [6, 10, 12, 13, 14, 15, 16]) and a composite with randomly distributed polygons (e.g. [15]). More appropriate three-dimensional models with randomly distributed spherical inclusions are researched in recent studies (e.g. [7, 15, 17, 18, 19, 20, 21]). However, to the authors' knowledge, there are no numerical studies focusing on debonding of ellipsoidal particles in composites with random microstructure.

In the present study, we focus on finite element (FE) modelling the large-strain mechanical behaviour of the HNBR-ZrW_2O_8 composite and validation of the numerical simulation against experiments. A multi-scale material modelling approach is used. Based on the optical analysis of particles images and microstructure images obtained by scanning electron microscope (SEM), realistic representative volume elements (RVE) of the microstructure are generated by using a novel algorithm developed in [22]. In the generated RVE, the shapes of the inclusions are approximated by prolate ellipsoids distributed randomly inside the RVE. The particle circularity and size distributions are taken into account. Then, the generated RVEs are transferred into ABAQUS [23] for subsequent non-linear finite element simulation to find out the overall mechanical properties of the composites. In the modelling approach, it is assumed that the mechanical behaviour of rubber is non-linear and described by the Marlow model [24]. The stiffness of ZrW_2O_8 is greater than that of rubber by a factor of 1000, therefore a linear behaviour of the filler material is assumed. The FE simulations are performed to reproduce uniaxial compression tests. Special attention is paid to the influence of the adhesive layer between matrix and particles on the effective mechanical properties.

The paper is structured in the following way. At the beginning, the material details and performed experiments are described. Next section is aimed to detail the RVE generation process for the FE simulation of the composites microstructure. Finally, simulation of uniaxial compression tests is performed for two limiting cases of the matrix-particle interface with perfect bond and no-adhesion. The stress-strain response given by simulations and experiments are then compared.

2. Materials and test methods

Composites of HNBR filled with various amount of zirconium tungstate up to 40 vol.% are prepared. The elastomer matrix material is based on HNBR with 96 % saturated polybutadiene with 36 % acrylonitrile content. A zirconium tungstate powder is obtained for the experiments from Alfa Aesar and used as a filler in HNBR [2]. The matrix material composition and manufacturing process of the composites were described in detail earlier in [2]. The microstructure of the composites is examined by scanning electron microscope (SEM) and optical microscopy. In addition, the filler particle size and circularity distributions are measured using a Malvern G3 Particle size analyser based on optical analysis of images of dispersed

particles at objective magnifications of 50, 10 and 2.5 [2].

The mechanical properties of the composite materials are investigated in a uniaxial compression mode using a Netzsch-Gabo Eplexor 150 DMTA machine with a 1.5 kN load cell and parallel plate specimen holders. For the experiments, button-shape specimens with 20 mm diameter and 10 mm height are produced by compression moulding. Smaller specimens of 10 mm diameter and 6 mm height are also employed due to the increased level of stiffness in HNBR with a high volume fraction of ZrW_2O_8. Silicone grease lubrication was employed to minimise barrelling. The investigated range of nominal compressive strains is 10-20 % which is relevant for rubber seals. The loading is performed stepwise with a nominal-strain step length of 5 % followed by a 3-hours stress relaxation period as in [25]. Prior to the experiments, the specimens were pre-treated with 4 full deformation cycles in order to minimise the Mullins effect [26] and left unloaded for at least 24 hours to restore the original shape.

3. Geometrical model of the microstructure

In order to accurately simulate the composite mechanical data, an adequate mathematical description of the actual filler inclusions in the composites is required. In the present work, we approximate the shape of the particles by prolate ellipsoids, see an example in Fig. 1. Despite the particles embedded into the HNBR matrix do not exactly resemble ellipsoids, such shape approximation can be justified by Hill's theorem [27]. The theorem suggests that a slightly uneven form of the particle surface has a minor effect on the overall elastic properties and, thereby, can be ignored (see discussion of this question in [28]).

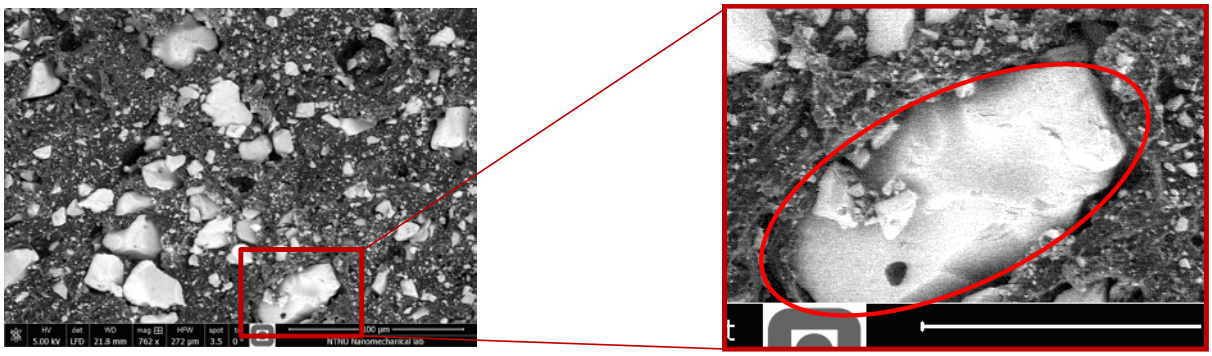

Fig. 1. The composite microstructure [2] and ellipsoidal approximation of the particle shape.

The microscopical image analysis of the particles enables to deduce their shape. In the analysis process, 3D particles are captured as a 2D image and two shape parameters are extracted from examination: circle equivalent (CE) diameter and circularity. CE diameter is the diameter of circle with an equivalent area in the 2D image. The particle circularity represents "closeness" of the particle shape to a perfect circle. The circularity is defined as follows:

$$Circularity = 4\pi A / P^2, \tag{1}$$

where A is the particle area; P is the particle perimeter. In case of the ellipsoidal approximation, the particle area is given by

$$A = \pi ab, \tag{2}$$

where a and b are the semi axes of ellipse. The ellipse perimeter could be calculated with help of the Ramanujan's approximation [29]

$$P = \pi(3(a+b) - \sqrt{(3a+b)(a+3b)}). \tag{3}$$

By substituting (2) and (3) into (1) and introducing aspect ratio $\gamma = a/b$, we obtain the following equation

$$Circularity = 4\gamma / (3(\gamma+1) - \sqrt{(3\gamma+1)(\gamma+3)})^2. \tag{4}$$

Equation (4) could be solved numerically for each value of circularity.

The particle size distribution obtained by the image analysis is shown in Fig. 2a and marked by a dotted line. The filler particles size takes values between 0.3 (defined by the instrument detection limit) and 12 μm. This interval is divided into 12 sections of equal length in order to create a geometrical model of RVE. The diameter of the particles is assumed to be constant in each of these sections. Thus, the non-linear distribution is approximated by a piece-wise linear function, given as a solid line in Fig. 2a. The same procedure is applied to the aspect ratio distribution, see Fig. 2b.

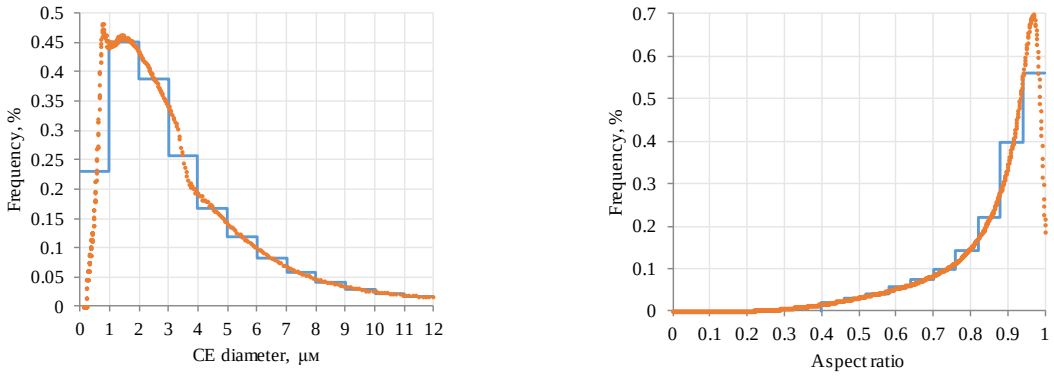

a) b)

Fig. 2. Particle circle equivalent (CE) diameter (a) and aspect ratio (b) distributions. Dotted lines represent the results of the particle image analysis, solid lines show piece-wise linear approximations.

It should be noted, that the particle shape analysis procedure does not allow to get both size and aspect ratio for each particle, i.e. it yields the overall distribution. Therefore, the following stochastic technique is applied to create a geometrical model of RVE. In accordance with the graphs shown in Fig. 2, two element arrays are created. The number of elements in the arrays is equal to the number of particles. The first array is supplied with values of the particle diameter in accordance with the particle size distribution (for instance, if an RVE consists of 100 particles, then 12 particles have a diameter of 0.5 μm and the first 12 elements of the array equal to 0.5 μm). The same method is used to fill the second array with values of the particle aspect ratio. Then, both arrays are combined randomly (for instance, the 25th element of the first array is combined with the 73rd element of the second array). Thus, the size and the shape of the particles can be considered stochastic. As an example, Fig. 3 illustrates an RVE with 100 particles for 17.3% and 35.8% of volume fraction. In the work, a novel algorithm for generation of (RVE) with randomly-oriented ellipsoidal filler particles of high volume fraction [22] is utilised.

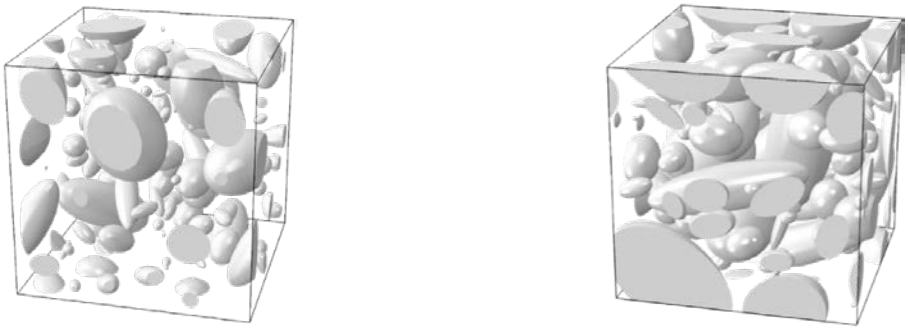

a) b)

Fig. 3. Examples of RVEs containing 100 particles with the size and shape distributions which correspond to the optical analysis of particle images. The volume fractions of filler are 17.3% (a) and 35.8% (b).

4. Effective mechanical properties

In addition to the filler inclusions, an accurate representation of the matrix behaviour is also necessary to obtain the effective properties and match the experimental stress-strain curves. It is assumed that the matrix material is incompressible with a non-linear behaviour described by the Marlow model [24]. The model is independent of the second strain invariant and based on the spline interpolation of the stress-strain data enabling exact representation of the stress-strain curve of rubber-like materials. An experimental stress-strain curve for uniaxial compression of the HNBR with a fitted line given by the Marlow model is shown in Fig. 4. The stiffness of ZrW_2O_8 is much larger than that of rubber (e.g. by a factor of 1000), therefore a linear behaviour of the filler material is assumed with the Young's modulus of 88.3 GPa and the Poisson's ratio of 0.3 [30].

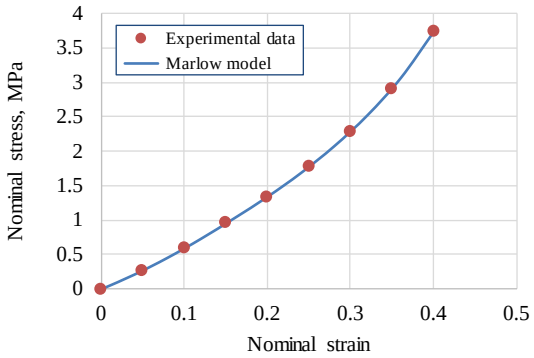

Fig. 4. Experimental stress-strain curve of the HNBR at uniaxial compression fitted by the Marlow model.

For finite element modelling, three RVEs for each volume fraction are created. Quadratic tetrahedral elements with hybrid formulation [23] are used for meshing. The averaged element size is equal to 0.05 in relation to the RVE edge. Averaged numbers of nodes and elements are about 300 000 and 200 000, respectively. The examples of FE models are shown in Fig. 5.

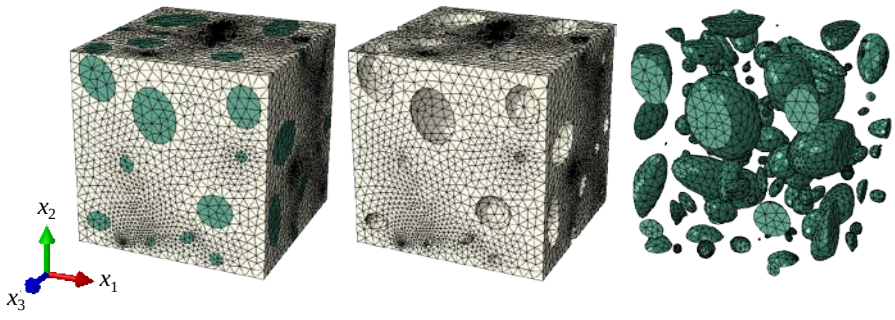

a)

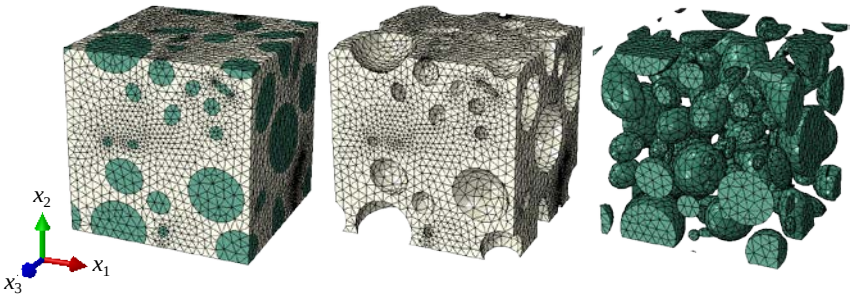

b)

Fig. 5. Examples of FE models of RVEs containing 100 particles with the volume fractions of filler 17.3% (a) and 35.8% (b).

The mechanical response of each RVE is not strictly isotropic because the finite number of particles is simulated. Therefore, we perform simulation of compression in three orthogonal directions, and then the results are averaged. For the compression in x_1 direction, the following boundary conditions (5) are applied:

$$\begin{aligned} &x_1 = 0: \quad u_1 = 0, \sigma_{12} = 0, \sigma_{13} = 0; \quad x_1 = L: \quad u_1 = -u_1^0, \sigma_{12} = 0, \sigma_{13} = 0; \\ &x_2 = 0: \quad u_2 = 0, \sigma_{12} = 0, \sigma_{23} = 0; \quad x_2 = L: \quad u_2 = \tilde{u}_2, \sigma_{12} = 0, \sigma_{23} = 0; \\ &x_3 = 0: \quad u_3 = 0, \sigma_{13} = 0, \sigma_{23} = 0; \quad x_3 = L: \quad u_3 = \tilde{u}_3, \sigma_{13} = 0, \sigma_{23} = 0, \end{aligned} \tag{5}$$

where u_1^0 is the applied displacement; $\tilde{u}_2$ and $\tilde{u}_3$ are unknown displacements defined during simulation, i.e. periodicity conditions are applied at faces $x_2 = L$ and $x_3 = L$. To obtain full stress-strain curves, the problem is solved with several linearly increasing values of u_1^0. As a result, we get stress and strain distributions for each value of u_1^0. The macroscopic stress and strain are then defined as the spatial averages (6):

$$\sigma_{11}^*(u_1^0) = \frac{1}{V}\int_V \sigma_{11} dV, \quad \varepsilon_{11}^*(u_1^0) = \frac{1}{V}\int_V \varepsilon_{11} dV. \tag{6}$$

Thus, the effective stress-strain curve in compression in x_1 direction is defined parametrically. The average stresses and strains in two other orthogonal directions are defined in the same manner.

For each volume fraction, stress-strain curves are obtained for three variants of RVE. The averaged stress-strain curves for both volume fractions are given in Fig. 6 with 95% confidence intervals together with experimental data. Experiments are performed for both filler volume fractions. As it can be seen, FE solutions yield higher values of stiffness in comparison with the experimental data for both volume fractions. This difference could be explained by damage of the interface between matrix and particles due to cycling pre-loading to large deformations. Such debonding, as it will be demonstrated below, in turn results in a considerable decrease in the composite stiffness.

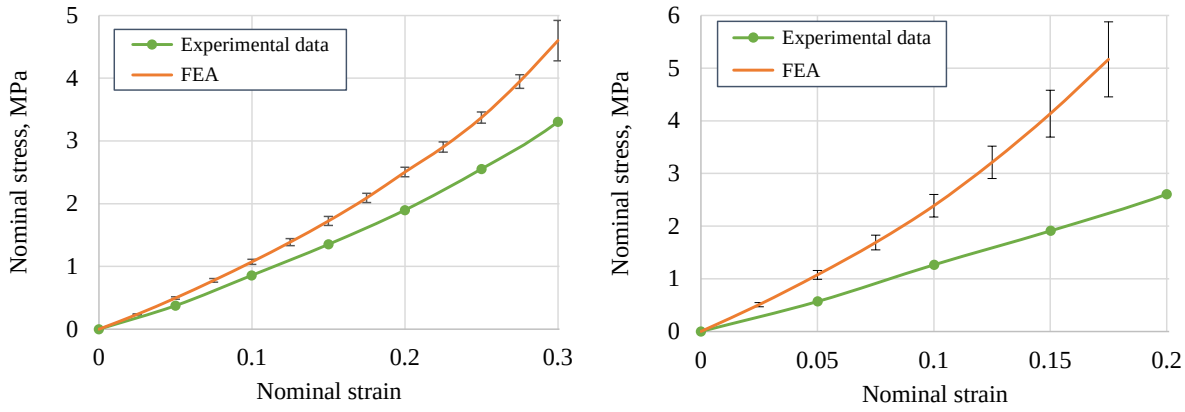

a) b)

Fig. 6. Stress-strain diagrams at uniaxial compression of HNBR-ZrW_2O_8 composites: FE analysis (FEA) and experimental data. The volume fractions of filler are 17.3% (a) and 35.8% (b).

5. Impact of particle-matrix interface on the effective mechanical properties

In the previous section, the matrix and particles are assumed to be perfectly bonded (i.e. the matrix and particles have shared nodes in the FE implementation). It might not be easy to achieve such conditions in real composites, if the interface is damaged at the production stage

or after pre-loading, especially to large deformations. It is well known, that the composite becomes softer when there is no adhesion between the matrix and its reinforcing particles. The interface, thus, plays a crucial role in the robustness of the final product. Therefore, this effect should be taken into account in large-strain applications.

Let us assume that adhesion is lost. To simulate the damaged interface, a contact interaction without friction between matrix and particles is applied. As in the previous section, compression in three orthogonal directions is modelled for various realizations of RVE with 17.3 and 35.8 vol.% of the filler inclusions. The deformed shapes of RVEs at various applied displacements are depicted in Fig. 7 and 8. It is clear, that the particles detach from matrix in the directions orthogonal to the compression direction manifesting voids occurring in the particle-matrix interfaces. The void growth progressively takes place with increasing longitudinal compressive deformation. Fig. 9 illustrates the results of FE simulations averaged over 3 simulation tests. Evidently, the FEA modelling results provide an interval which enclose the experimental data. Thus, it could be concluded, that the interface between particles and the matrix is partially damaged in the studied pre-loaded specimens which is manifested in a significant decrease of stiffness. For instance, the stress response in the composite with 35.8 vol.% of filler with intact interface subjected to the nominal compressive strain of 0.175 is about two times greater than that in the composite with a damaged interface. Comparison of experimental and modelling results shows that the level of interface damage depends on the volume fraction. For 17.3 vol.% of the filler, the experimental stress-strain curve is between the bounds given by FE simulations, while for 35.8 vol.%, experimental data are closer to the modelling results with no-adhesion. The point is that higher filler volume fraction leads to a higher stress level at particle-matrix interfaces, and, therefore, a higher damage level of the interfaces.

It should be noted that the performed FE simulation gives the lower and upper bounds for the effective finite-strain properties of the composite: the upper bound corresponds to a perfect particle-matrix interface is considered, while the damaged interface provides the lower bound. The proposed approach is important for the industrial applications of composites giving a range of the effective properties. Hence, the performance of composites could be analysed taking various levels of debonding into account. Note also, that estimation of the damage level in the composite (at least qualitatively) is possible if compare experimental results with the theoretical bounds of stiffness at finite strains with the ideal and fully damaged interfaces.

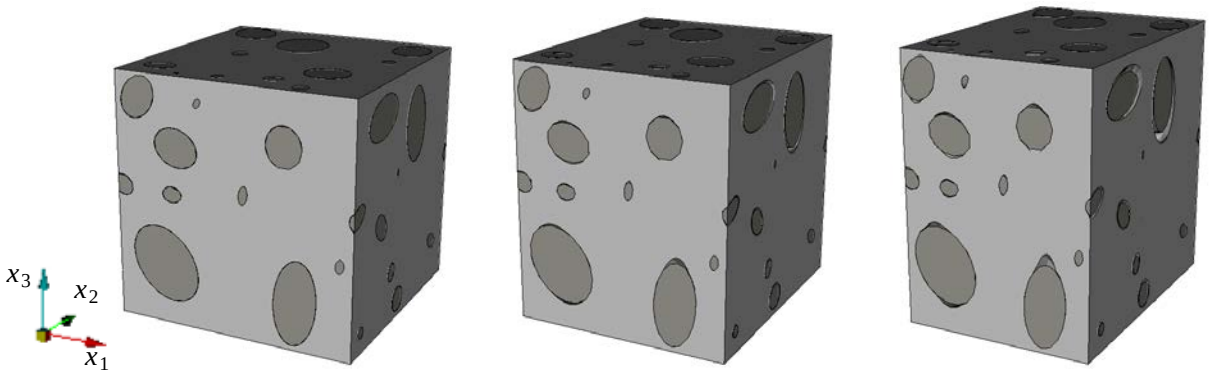

Fig. 7. The original and deformed shapes of RVE with 17.3 vol.% of filler due to uniaxial compression in x_1 direction.

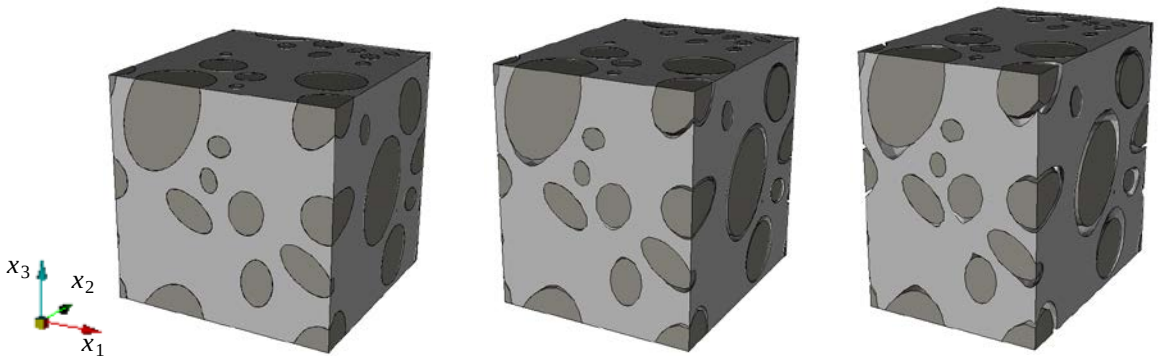

$u_1^0 = 0 \times L$ $u_1^0 = 0.1 \times L$ $u_1^0 = 0.2 \times L$

Fig. 8. The original and deformed shapes of RVE with 35.8 vol.% of filler due to uniaxial compression in x_1 direction.

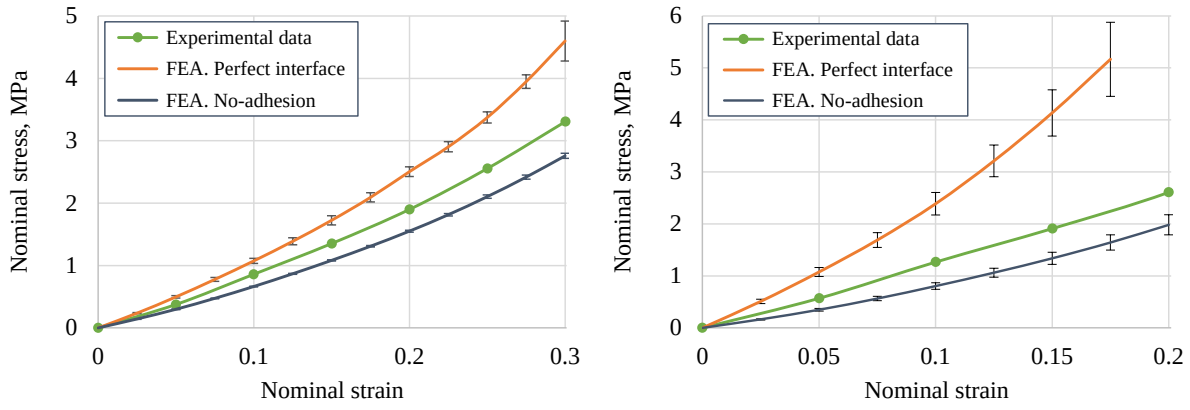

a) b)

Fig. 9. Stress-strain diagrams at uniaxial compression of HNBR-ZrW_2O_8 composites: FE analyses (FEA) for two the types of interaction between matrix and particles (Perfect interface and No-adhesion) and experimental data (Test 1, 2). The volume fractions of filler are 17.3% (a) and 35.8% (b).

6. Summary and concluding remarks

The paper aims to study the mechanical behaviour of composites made of hydrogenated nitrile butadiene rubber (HNBR) and particles of zirconium tungstate ZrW_2O_8 prepared with various tungstate volume fractions. Microstructure of the composites was studied by scanning electron microscope (SEM), and the particle shape parameter distributions were computed using optical analysis of the images of dispersed tungstate particles. The composites were subjected to cycling pre-loading to remove the Mullins effect prior to the main mechanical experiments.

The behaviour of the composites was studied at uniaxial compression experimentally and simulated by a micro-mechanical approach using finite element method (FEM). In the work, a novel algorithm for generation of representative volume element (RVE) with randomly-oriented ellipsoidal filler particles of high volume fraction was utilised. Based on measured size and aspect ratio distributions, three RVEs containing 100 randomly distributed ellipsoidal particles were generated for both 17.3% and 35.8% of filler volume fractions and further used in FE simulations. The non-linear stress-strain behaviour of HNBR was accurately reproduced by the Marlow model, while rigid particles were assumed linear elastic. Two limiting cases of a contact interaction between matrix and particles were considered: a perfect interface and the absence of the adhesive bonding between filler and matrix.

The investigation of the mechanical behaviour of the composites began with an

assumption that the interfacial layer between particles and matrix is intact. We showed that the FEM predictions of the effective stress-strain curves do not correspond to the experimental data for the composites: the FE simulations yield a stiffer response than the real composite material actually exhibits. We believed that the reason of the material softening is debonding of the filler inclusions from the matrix due to the cycling pre-loading performed before the uniaxial compression tests. As we had showed earlier [1], mechanical loading could lead to a large strain at the interface between particles and matrix, therefore the cycling loading could have damage the interface. In order to verify this hypothesis, interaction between matrix and particles was changed to the "no-adhesion" condition. For this interaction model, FE simulation demonstrates a decrease of the effective stiffness of the composites. Two limiting cases of the interface modelling provide bounds for real effective properties of the composites at finite strains. It was also shown that the damage level increases with increasing filler volume fraction.

In the modelling approach, it was assumed that all particles are either perfectly interacted with the matrix or debonded from the matrix. For further investigation of the problem, it would be interesting to incorporate the cohesive-zone model [31, 32] to simulate the damage accumulation process in the filler-matrix interface with progressive deformation and also cycling loading. It should also be noted that the ZrW_2O_8 particles used here are not pretreated, whereas surface modification of ZrW_2O_8 has been reported [33, 34] to improve interaction with different polymer matrices. Therefore, it would be interesting to research the effect of a particle pretreatment on the mechanical properties and the degree of debonding at finite strains.

Acknowledgements

This work was supported in part by the Research Council of Norway (Project 234115 in the Petromaks2 programme). The first and third authors acknowledge the financial support from the Russian Foundation for Basic Research (Grant No. 16-01-00815). We thank Ben Alcock and Christelle Denonville at SINTEF Materials and Chemistry for the measurement of ZrW_2O_8 particle size and circularity distribution.

References

[1] S.N. Shubin, A.B. Freidin, A.G. Akulichev // *Archive of Applied Mechanics* **86** (2016) 351.
[2] A.G. Akulichev, B. Alcock, A. Tiwari, A.T. Echtermeyer // *Journal of Materials Science* **51** (2016) 10714.
[3] R.F. Robbins, Y. Ohori, D.H. Weitzel // *Rubber Chemistry and Technology* **37** (1964) 154.
[4] A.G. Akulichev, A.T. Echtermeyer, B.N.J. Persson // *International Journal of Pressure Vessels and Piping* (2017). doi: 10.1016/j.ijpvp.2017.11.014
[5] A.N. Gent, B. Park // *Journal of Materials Science* **19** (1984) 1974
[6] P.A. Toulemonde, J. Diani, P. Gilormini // *Mechanics of Materials* **93** (2016) 124.
[7] P. Gilormini, P.-A. Toulemonde, J. Diani // *Mechanics of Materials* **111** (2017) 57.
[8] P.-A. Toulemonde et al. // *Journal of Materials Science* **52** (2017) 878.
[9] A.P.S. Selvadurai // *Continuum Mechanics and Thermodynamics* **28** (2016) 617.
[10] H.M. Inglis et al. // *Mechanics of materials* **39** (2007) 580.
[11] X.A. Zhong, W.G. Knauss // *Journal of Engineering Materials and Technology* **119** (1997) 198.
[12] J. Moraleda, J. Segurado, J. Llorca // *International Journal of Solids and Structures* **46** (2009) 4287.
[13] L. Yang et al. // *Composites Science and Technology* **72** (2012) 1818.
[14] P. A. Toulemonde et al. // *Matériaux et Techniques* **103** (2015) 306-1-7.
[15] H. Arora et al. // *Computational Materials Science* **110** (2015) 91.
[16] L. Riaño, L. Belec, Y. Joliff // *Composite Structures* **154** (2016) 11.
[17] K. Matous, P.H. Geubelle // *Computer Methods in Applied Mechanics and Engineering*

196 (2006) 620.
[18] K. Matous et al. // *Composites Science and Technology* **67** (2007) 1694.
[19] D. Sodhani, S. Reese // *Macromolecules* **47** (2014) 3161.
[20] D.W. Spring, G.H. Paulino // *Computational Materials Science* **109** (2015) 209.
[21] Y. Cho et al. // *Materials* **10** (2017).
[22] S.N. Shubin, A.B. Freidin // *PNRPU Mechanics Bulletin* **4** (2016) 317.
[23] Abaqus, *Dassault Systemes Simulia Corporation* (Providence, RI, USA, 2012).
[24] R.S. Marlow, In *Constitutive Models for Rubber III* (UK, AA Balkema Publishers, 2003), 157
[25] A.G. Akulichev, B. Alcock, A.T. Echtermeyer // *Polymer testing* **63** (2017) 226.
[26] L. Mullins // *Rubber Chemistry and Technology* **42** (1969) 339.
[27] R. Hill // *Journal of the Mechanics and Physics of Solids* **11** (1963) 357.
[28] M. Kachanov, I. Sevostianov // *International Journal of Solids and Structures* **42** (2005) 309.
[29] G.H. Hardy, A.P.V. Seshu, B.M. Wilson, *Collected papers of Srinivasa Ramanujan* (Cambridge University Press London, Fetter Lane, 1927).
[30] F.R. Drymiotis et al. // *Physical Review Letters* **93** (2004) 059903.
[31] K. Park, G.H. Paulino // *Applied Mechanics Review* **64** (2011) 060802-1.
[32] D.W. Spring, O. Giraldo-Londono, G.H. Paulino // *Mechanics Research Communications* **78** (2016) 100.
[33] C. Lind et al. // *Physica Status Solidi B* **1** (2011) 123.
[34] L.M. Sullivan, C.M. Lukehart // *Chemistry of Materials* **17** (2005) 2136.